Numerical computation of turbulent flow through a square-sectioned 90° bend

H. Iacovides, B. E. Launder, and P. A. Loizou*

Finite-volume, semi-elliptic computations are reported of the three-dimensional flow around a 90° square-sectioned bend for which detailed laser-Doppler measurements have been reported by Taylor *et al.*[1] While the standard k-ε eddy-viscosity model has been used in the main flow region, in place of the usual "wall functions," the mixing-length hypothesis has been employed to resolve the flow in the layer immediately adjacent to the wall. The scheme is successful in predicting the details of the primary and secondary flow fields both within the bend and downstream thereof.

Keywords: *flow computation, turbulent flow, square-sectioned bend*

Introduction

The flow in bends of rectangular cross section provides a well-defined, strongly three-dimensional flow field with close generic similarities with those arising in turbomachine blade passages. Extensive LDA studies of the development of flow around 90° bends of uniform cross section have been reported by the Fluids Section at Imperial College (Taylor *et al.*,[1] Humphrey *et al.*,[2] Enayet *et al.*,[3] whereas Chang *et al.*[4] have reported corresponding measurements for flow in a 180° U-bend.

The last of these experiments has been the subject of several attempts at numerical simulation. The initial efforts were so unsuccessful that by 90° around the bend, the computed and measured flow fields bore little resemblance to one another (Chang *et al.*,[5] Johnson,[6] Birch[7]). Recently, however, Choi *et al.*[8] obtained results for that flow, using the standard k-ε model, that, though still exhibiting significant differences from the experiment at 90°, represented a marked improvement on the results of earlier studies. The improvement stemmed principally from the abandonment of "wall functions" for handling the region immediately adjacent to the wall. Instead of these overall "resistance" formulas, a sufficiently fine grid was used near the walls to resolve the changeover from turbulent to viscous transport by way of a low Reynolds number turbulence model. A version of Prandtl's mixing-length hypothesis was used to approximate the turbulent transport processes across this sublayer; despite the simplicity of this prescription, it has been used successfully in several studies of turbulent flow near spinning discs and cylinders,[9,10] where, as in the bend flow, the ratio of secondary to primary velocities changes rapidly across the viscosity-affected sublayer.

The 180° bend flow of Chang *et al.* provided a very severe test of the computational procedure, but it was arguably not one that was especially close to the flows arising in blade passages. This was because the flow was nearly fully developed at entry to the bend, a situation giving rise to a very strong, multicellular secondary flow. The experiment reported by Taylor[1] provided a more directly relevant test flow for blading situations: The boundary layers at entry to the 90° bend were only some 15% of the passage dimension, whereas the ratio of mean radius of curvature to hydraulic diameter of 2.3:1 was 50% less than in Chang.[4] Kreskovsky *et al.*[11] have, in fact, already reported computations of this flow employing a simple mean-field closure for the Reynolds stresses. The level of agreement achieved was fairly good, though there was insufficient growth of the boundary layer on the convex inner surface toward the end of the bend where the flow on that surface encountered a substantial adverse pressure gradient. This paper addresses whether the two-equation turbulent transport model used in Choi[8] would lead to a marked improvement in the numerical simulation of Taylor's experiment over that previously obtained.

* Department of Mechanical Engineering, The University of Manchester Institute of Science and Technology, Manchester, M60 1QD, United Kingdom

Received 15 October 1986 and accepted for publication 19 January 1987

0142-727X/87/040320-06$03.00

Numerical and physical model

The numerical solver employed for the computations is of finite-volume type. It solves on the usual staggered velocity-pressure grid the discretized, three-dimensional Reynolds equations in cylindrical polar coordinates. A semi-elliptic solution strategy, Pratap and Spalding,[12] is adopted in which only the pressure field is stored over the whole domain. Other variables are held only on two adjacent planes, their values being continually overwritten as successive iterative upstream-downstream sweeps are made around the bend. The methodology is broadly patterned on the TEACH family of computer programs developed by Gosman at Imperial College.[13] The main elements of the procedure have been reported in several earlier publications[8,14] and in greater detail by Iacovides.[15] Here, therefore, we note simply that

- The nondiffusive QUICK scheme[16] is used for discretizing convective transport in the cross section of the duct.
- Both the SIMPLER[17] and SIMPLE[18] algorithms are used at different stages of the solution for correcting the pressure field to bring compliance with continuity (the former during the initial stages when residuals are large).
- While initially finite-difference coefficients are evaluated from flow data at the upstream plane, as convergence is approached first one then two in-plane iterations are made. This important step was not included in the original computations of Pratap,[12] who confined attention to bends of larger radius ratio.
- While the standard k-ε eddy viscosity model of turbulence[19] is applied over nearly all the flow, within a band of thickness $0.04D_H$ adjacent to the walls, the turbulent viscosity is obtained from Van Driest's[20] form of the mixing-length hypothesis generalized for three-dimensional flows:

$$\nu_t = \ell_m^2 \left[\frac{\partial U_i}{\partial x_j} \left(\frac{\partial U_i}{\partial x_j} + \frac{\partial U_j}{\partial x_i} \right) \right]^{1/2}$$

The mixing length ℓ_m is given by

$$\ell_m = 0.419 x_n \left(1 - \exp - \frac{x_n \tau_w}{26\nu} \right)$$

where x_n denotes the distance of a point from the (nearest) wall, and τ_w is the local (resultant) wall shear stress at the closest point on the wall.

In matching this model to the k-ε EVM at the edge of this sublayer, the values of k and ε were fixed by requiring that the turbulence energy dissipation and production rates be in balance and that the turbulent viscosities given by the two models be equal.

Unfortunately, one practice that proved very beneficial to our earlier computations in *circular* sectioned bends had to be discarded in these square bend computations. For the circular bends, the small variation in static pressure across the near-wall sublayer was neglected,[14] which meant that the fine grid needed to resolve the changeover from turbulent to viscous transport could be included without significantly increasing the overall core demand (which was mainly fixed by the size of the three-dimensional pressure array). Although several variants of this practice were explored, none could be found that was satisfactory for ducts of square cross section, the problem being that, in the corners, pressure gradients normal the wall are necessarily large to make the strong secondary flow change direction by 90°. Fortunately, the growth in computer memory available has meant sufficient core has been accessible to extend the pressure domain over the near-wall sublayer as well as the fully turbulent part of the flow.

Computational details and results

The computations reported have used a 25×47 mesh to cover the half cross section of the duct between the symmetry plane and the end wall (Figure 1). Eight nodes have been assigned to the near-wall regions, where the mixing-length hypothesis is used. Over the remainder of the cross section, internode spacing increased smoothly with distance from the wall. The nonuniformity of the mesh is greater than that used by Choi[8] to compute the 180° bend with fully developed entry conditions. The thinner inlet boundary layers of the present flow demanded that a greater proportion of the nodes be placed near the walls to properly resolve the growth of the boundary layer during the initial stages of development.

Computations began 2.5 diameters upstream of the bend using profiles of mean velocity and turbulence variables (k and ε) generated in a separate computation of developing turbulent flow in a straight duct. The precise boundary layer thickness at the $-2.5D_H$ position was not known, but computations were initiated with slightly different inlet profiles until optimum agreement was achieved with the measured streamwise velocity profile at 0.25 diameters upstream of the bend. In the calculations, dependent variables were evaluated on 135 cross-sectional planes, 18 of which were upstream of the bend, 40 downstream, and 77 in the bend itself.

Over the first 30° of the bend, viscous effects are fairly weak, boundary layers remain thin, and computations of Kreskovsky *et al.*[11] achieve just as satisfactory agreement with the experimental data of Taylor *et al.*[1] as do the present ones. However, by 60° (Figure 2), significant differences have begun to develop near the inside of the bend ($r^* = 0.9$), where the present model predicts a stronger secondary velocity, V, and a primary (streamwise) velocity that reaches its maximum value at $x^* \simeq 0.3$ rather than at the symmetry plane. Both features are in accord with the experimental data. At 77.5°, similar but larger differences are evident between the two computations (Figure 3), and again the present computations closely agree with the measured profiles. Indeed, consistently better agreement with the measured primary velocity occurs for each of five constant-r^* traverse lines along which the data were gathered. Figure 4 presents for the same station axial velocity contours and secondary flow vectors. These show how the secondary flow current causes the streamwise velocity along $r^* = 0.9$ to be so low in the vicinity of the symmetry plane. In the corner of the convex wall, a small secondary recirculation is just visible, though it has no perceptible effect on the streamwise flow pattern.

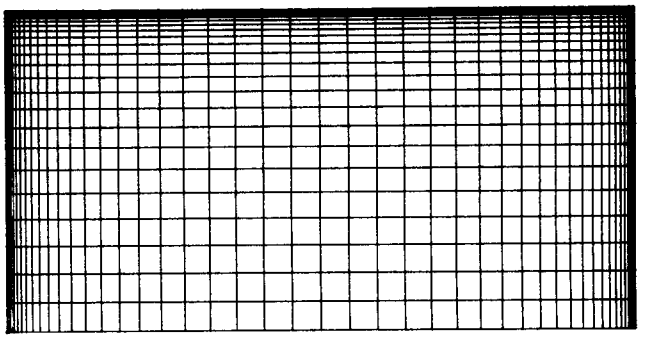

Figure 1 Distribution of mesh lines over the computational domain

No further results were shown by Kreskovsky *et al.*,[11] but since experimental data are reported at 0.25 and 2.5 hydraulic diameters downstream of the bend, these are compared with the present computations in Figures 5 and 6. At both positions, agreement with experiment is extremely close, the slowly decaying secondary flow downstream of the bend being particularly well predicted. A further view of the secondary flow at $2.5D_H$ is provided in Figure 7, where the secondary flow vectors are shown alongside contours of axial velocity. Because the secondary flow persists downstream of the bend, the streamwise velocity contours undergo continued deformation to the convoluted pattern of Figure 7. The corner secondary recirculation noted at 77.5° has grown somewhat but remains an essentially passive feature of the flow. A major and probably crucial difference between this flow and the 180° bend computed with less sucess by Choi *et al.*[8] is that, in the latter case, the secondary motion (according to the predictions) breaks down into multiple counter-rotating eddies (Figure 8); it is likely that in the actual experiment the secondary flow pattern was even more complex.

Notation

D_H	Hydraulic diameter, defined as 4 × cross-sectional area/wetted perimeter
k	Turbulent kinetic energy
r^*	Normalized radial coordinate $= \left(\frac{R_{out} - r}{R_{out} - R_{in}}\right)$
R_{in}	Inner side wall radius of curvature
R_{out}	Outer side wall radius of curvature
V	Radial direction velocity component
W	Streamwise direction velocity component
W_b	Bulk fluid velocity in streamwise direction
x^*	Spanwise coordinate normalized by $\frac{D_H}{2}$
x_n	Distance of a point from nearest wall
ε	Turbulence energy dissipation rate
ℓ_m	Mixing length
ν_t	Turbulent viscosity
ρ	Density of fluid
τ_w	Wall shear stress

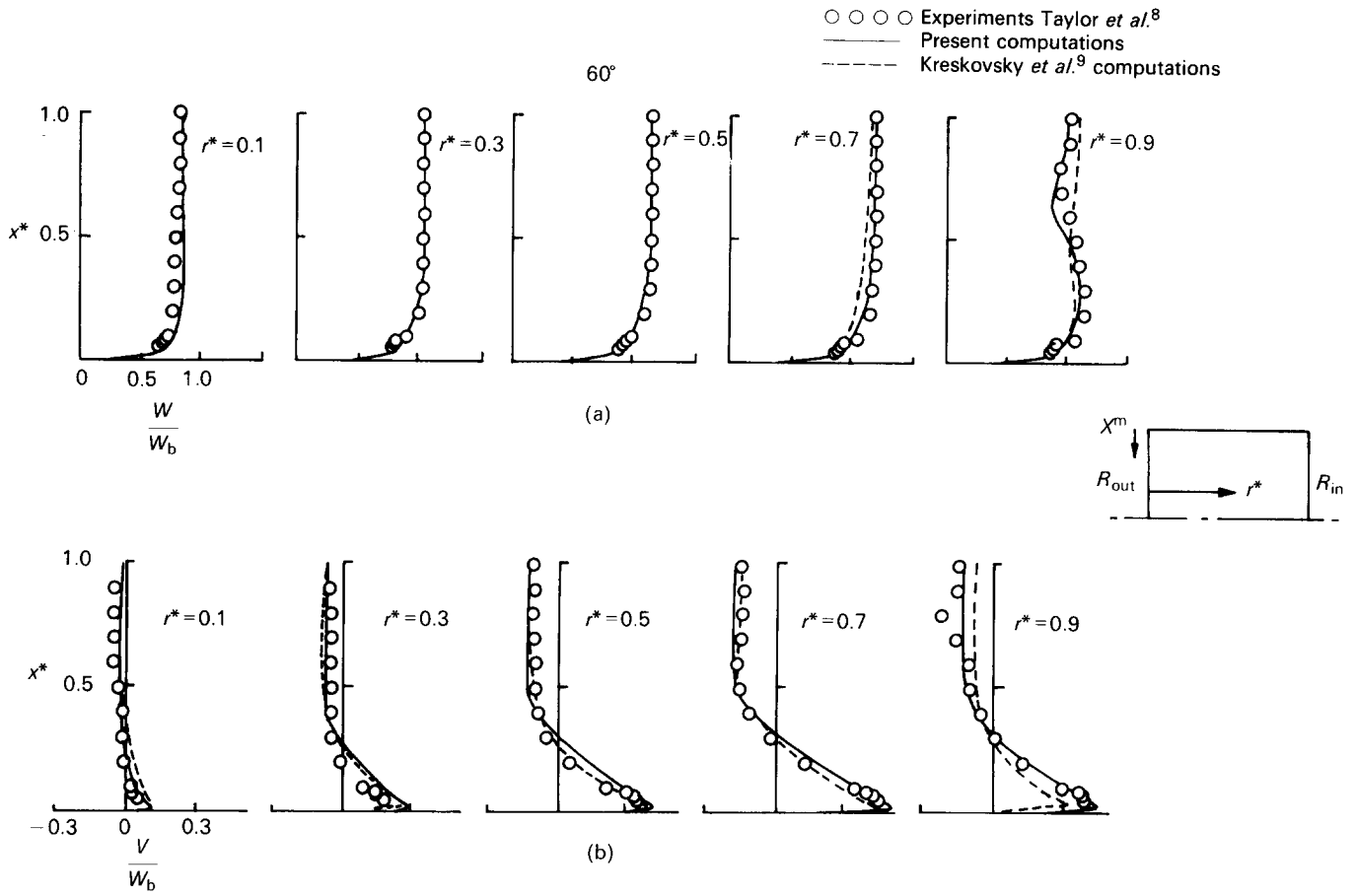

Figure 2 Mean velocity profiles at 60° around the bend: (a) streamwise velocity profiles; (b) radial velocity profiles

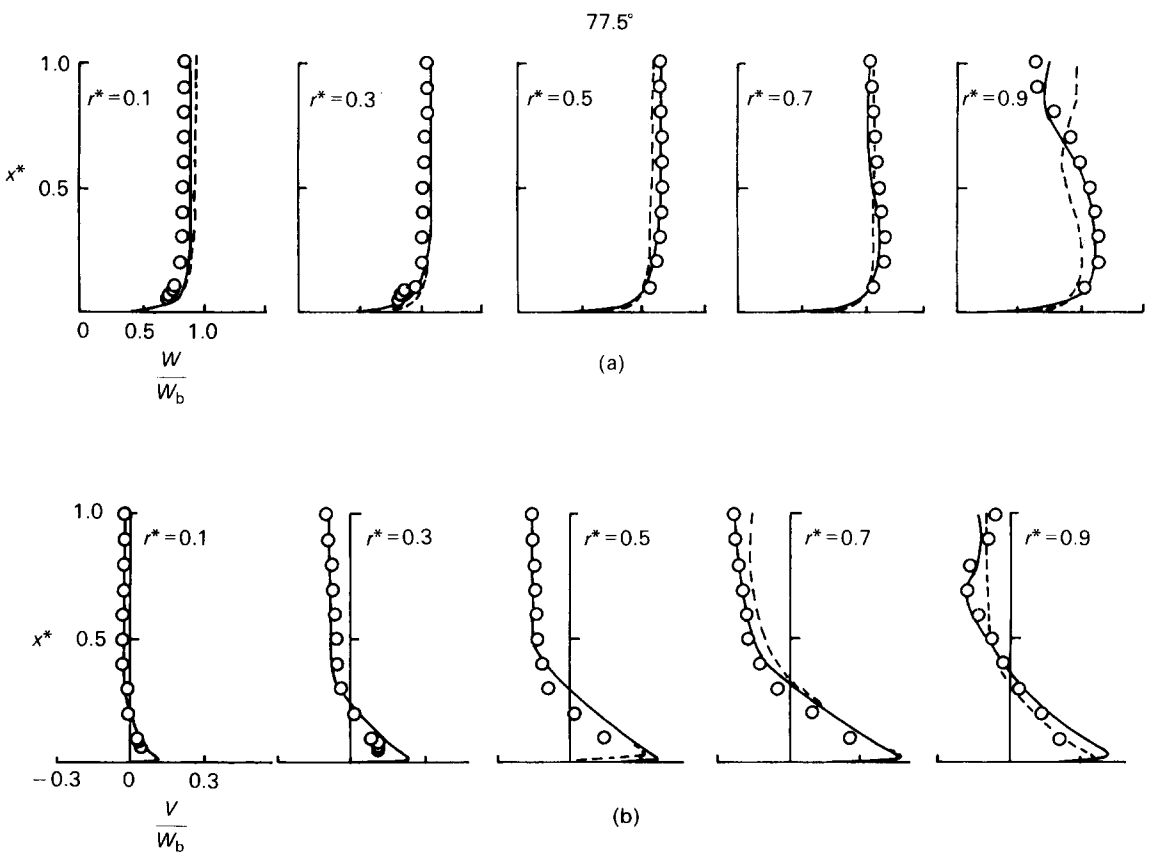

Figure 3 Mean velocity profiles at 77.5° around the bend: (a) streamwise velocity profiles; (b) radial velocity profiles

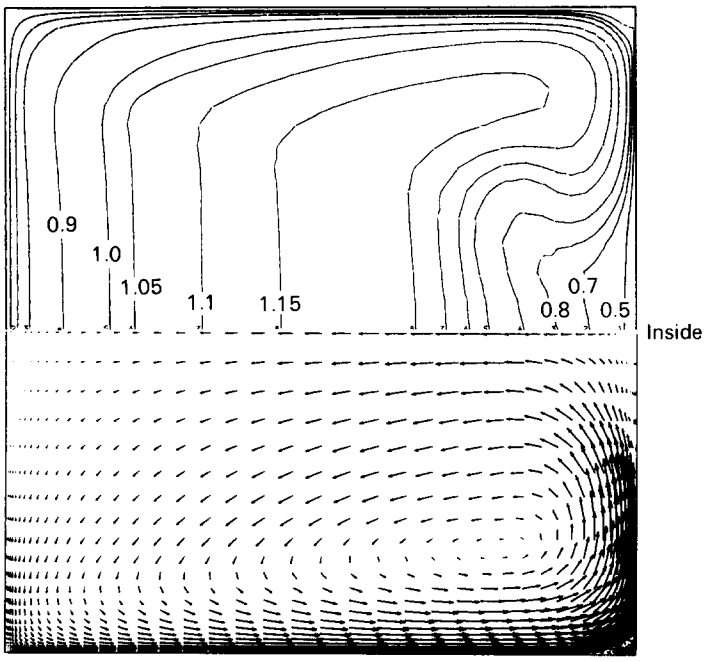

Figure 4 Computed axial velocity contours (W/W_b) and secondary flow vectors at 77.5° around the bend

The computed variation of wall friction is shown in Figure 9 along four lines: the lines of symmetry on the concave and convex walls and the lines on the same walls at a distance $0.03D_H$ from the end wall. On the concave surface, the friction factor drops abruptly just ahead of the bend because of the flow shifting to the inside. The consequent adverse pressure gradient on the outside of the bend almost produces reverse flow in the corner (line *D*). Just before outlet, it is the convex wall boundary layer that suffers an adverse pressure gradient, and here it is the boundary layer on the symmetry plane that comes perilously close to separation. The reason the risk of separation at outlet is greater at the midplane than in the corner is that it is there that the secondary flow "dumps" the fluid with the lowest axial momentum. It appears that the choice of bend radius ratio has been well chosen so as just to avoid separation at both inlet and exit.

Conclusion

Numerical simulation of the strongly three-dimensional turbulent shear flow arising in flow around a 90° bend of small radius ratio has achieved excellent agreement with experiment. The turbulent stresses have been approximated by the standard k-ε EVM over most of the flow, and the mixing-length hypothesis is used to extend computations across the semiturbulent and viscous sublayers to the wall. This hybrid

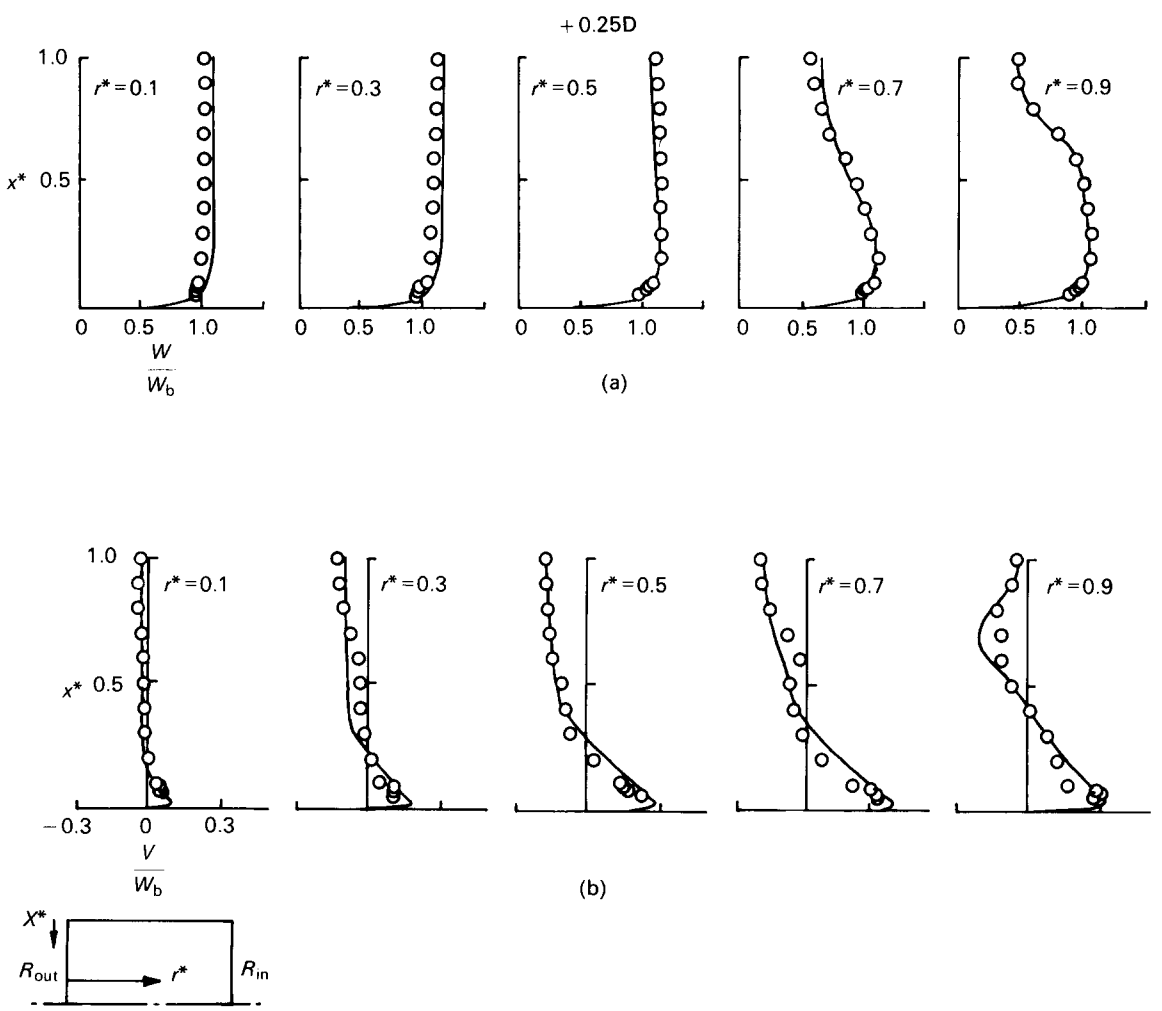

Figure 5 Mean velocity profiles at 0.25 hydraulic diameters downstream of the bend: (a) streamwise velocity profiles; (b) radial velocity profiles

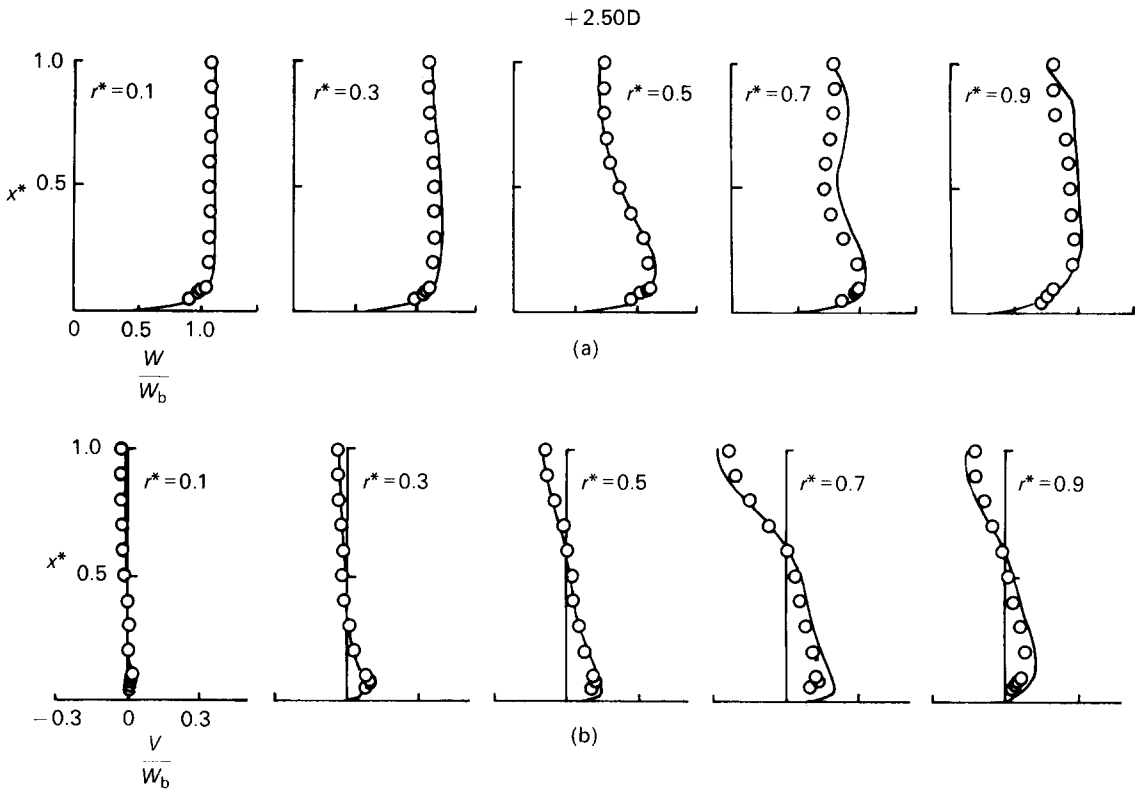

Figure 6 Mean velocity profiles at 2.5 hydraulic diameters downstream of the bend: (a) streamwise velocity profiles; (b) radial velocity profiles

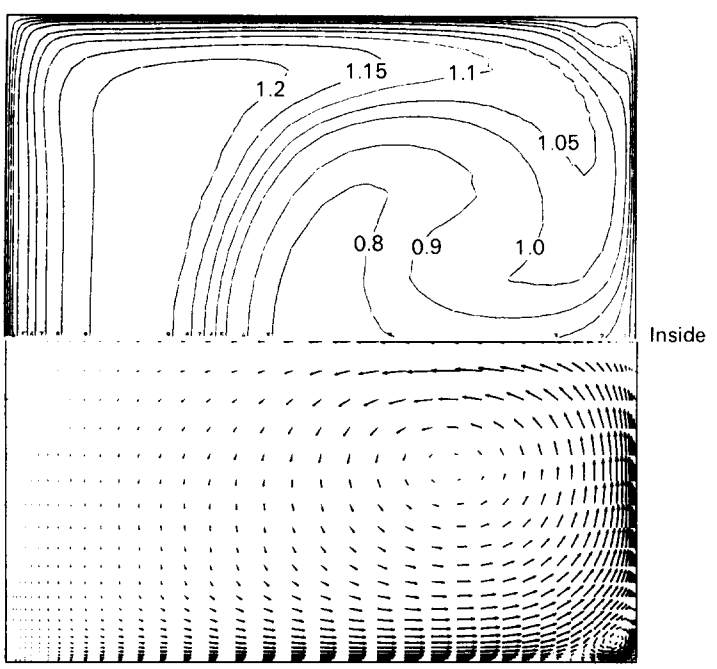

Figure 7 Computed axial velocity contours (W/W_b) and secondary flow vectors at $2.5D_H$ downstream of the bend

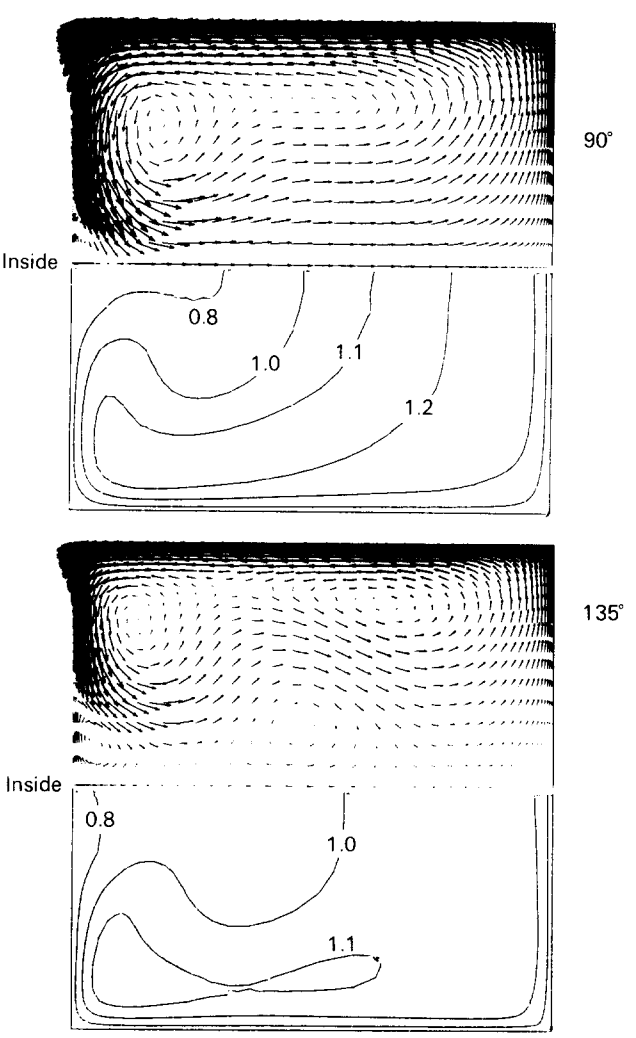

Figure 8 Axial velocity contours and secondary flow vectors in 180° bend with thick inlet boundary layers (from Choi *et al.*)

model achieves significantly better agreement than when a mean field closure is used over the whole field, and it almost certainly does better than matching the k-ε model to wall functions. Although experience indicates that a second-moment closure should allow more reliable predictions at the expense of (considerably) more computational effort, in many blading situations where the shear layers remain fairly thin it is doubtful whether the additional effort could be justified.

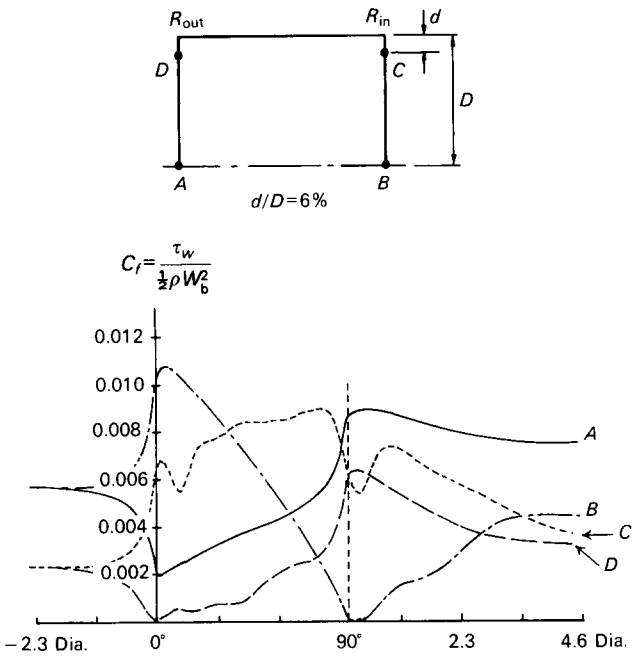

Figure 9 Development of wall friction coefficient around the bend along four reference lines

Acknowledgements

Initial funding for the project was provided by NASA Lewis under contract NAGW-779. During the final stages, Mr. P. A. Loizou was supported jointly by Rolls-Royce plc and the SERC through grant GR/D65367. The software used in the study was converted from an existing code for toroidal geometries with the support of Rolls-Royce Bristol under brochure 2D2/52B.

References

1 Taylor, A. M. K. P., Whitelaw, J. H., and Yianneskis, M. *J. Fluids Eng., Trans. ASME*, 1982, **104**, 350.
2 Humphrey, J. A. C., Whitelaw, J. H., and Yee, G. *J. Fluid Mech.*, 1981, **103**, 443.
3 Enayet, M. M., Gibson, M. M., Taylor, A. M. K. P., and Yianneskis, M. *Int. J. Heat and Fluid Flow*, 1982, **3**, 221.
4 Chang, S. M., Humphrey, J. A. C., and Modavi, A. *Physico-Chemical Hydrodynamics*, 1983, **4**, 243.
5 Chang, S. M., Humphrey, J. A. C., Johnson, R. W., and Launder, B. E. *Proc. 4th Turbulent Shear Flows Symposium*, 6.20–6.25, Karlsruhe, 1983.
6 Johnson, R. W. Turbulent convecting flow in a square duct with a 180° bend: an experimental and numerical study. PhD thesis, Faculty of Technology, University of Manchester, 1984.
7 Birch, N. The calculation of 3D flow in curved ducts using Q385. *Rolls-Royce Theoretical Sciences Group*, Derby, rep. no. TSG 0161, 1984.
8 Choi, Y-D, Iacovides, H., and Launder, B. E. Submitted to *ASME J. Fluids Eng.*, 1986.
9 Koo, S. L., Launder, B. E., and Sharma, B. I. *ASME J. Heat Trans.*, 1974, **96C**, 204.
10 Sharma, B. I., Launder, B. E., and Scott, C. J. *ASME J. Fluids Eng.*, 1976, **98**, 753.
11 Kreskovsky, J. P., Briley, W. R., and McDonald, H. Prediction of laminar and turbulent primary and secondary flows in strongly curved ducts. NASA rep. no. CR-3388, 1981.
12 Pratap, V. S., and Spalding, D. B. *Aero. Quart.*, 1975, **26**, 219.
13 Gosman, A. D., and Ideriah, F. J. K. TEACH-2E: a general computer program for two-dimensional, turbulent, recirculating flows. Mech. Eng. Dept. Rep., Imperial College, London, 1976.
14 Iacovides, H., and Launder, B. E. *Proc. 4th Int. Conf. on Numerical Methods in Laminar and Turbulent Flow*, 1023–1045, Swansea, 1985.
15 Iacovides, H. Momentum and heat transport in flow through 180° bends of circular cross section. PhD thesis, Faculty of Technology, University of Manchester, 1986.
16 Leonard, B. P. *Comp. Methods Appl. Eng.*, 1979, **19**, 59.
17 Patankar, S. V. *Numerical Heat Transfer and Fluid Flow*, Hemisphere, New York, 1980.
18 Patankar, S. V., and Spalding, D. B. *Int. J. Heat Mass Transfer*, 1972, **15**, 1787.
19 Launder, B. E., and Spalding, D. B. *Comp. Methods in Appl. Mech. and Eng.*, 1974, **3**, 269.
20 Van Driest, E. R. *J. Aero. Sci.*, 1956, **23**, 1007.